Optics in Remote Sensing

Thomas Walther and Edward S. Fry

T. Walther
Institute for Applied Physics, TU Darmstadt, Schlossgartenstr. 7, D-64289 Darmstadt, Germany

E.S. Fry (✉)
Department of Physics and Astronomy, Texas A&M University, College Station, TX 77843-4242, USA
e-mail: fry@physics.tamu.edu

M.D. Al-Amri et al. (eds.), *Optics in Our Time*, DOI 10.1007/978-3-319-31903-2_9

9.1 Introduction

The observation of light or more specifically the difference between day and night is the very first encounter of physics every human experiences at a very early stage in life. So not surprisingly, optics and the study of the properties of light is one of the oldest in the history of science. The concept of straight propagation of light in homogenous media dates back to the ancient Greeks. This is known as Hero's principle. Although we have learned a lot about light throughout the centuries and have discovered more subtle effects about how light propagates, Hero's principle is the most important feature when applying light to remote sensing. However, we will see that despite its relative early beginnings, modern remote sensing is intimately connected with modern tools of optics such as pulsed lasers, fast detectors, etc.

Optical remote sensing involves the use of light to observe distant objects and to obtain parameters or characteristics of those objects; it can be passive or active. Passive remote sensing would include seeing the light emitted by the object, e.g., a star, the sun, or even the headlights of an approaching car. Remote sensing in the latter case enables one to determine the location of the car and whether it may be on a collision course. Passive remote sensing would also include seeing an object, but via the light from some other source that is scattered/reflected by it; examples include seeing the moon and the planets via the light from the sun that is scattered by them, or just a boy standing in the street and illuminated by the afternoon sun. In either case the light scattered or emitted by the object can also be analyzed to determine some properties of the object; examples include the color of the object and how fast it is moving towards or away from you.

Active remote sensing involves sending out a beam of light and observing the light reflected or scattered by an object. A simple example would be the headlights of a car that illuminate a girl running across the street at midnight. Active remote sensing using a laser to illuminate the object is a technique named LIDAR, a name that arises from a linguistic blend of light and radar. In analogy with the term radar, one might say that it is an acronym for "LIght Detection And Ranging"; but there is no consensus and one can frequently find other definitions such as "Laser Imaging, Detection And Ranging," or "Light Intensity Distance And Ranging." In addition, there is no consensus that it should be an acronym with all capital letters; consequently, it is also variously referenced in publications as LiDAR, Lidar, or just lidar.

This contribution aims at outlining how light is used in remote sensing. First, a short historical overview of remote sensing will be given. This introduction is followed by some of the technical developments leading to modern remote sensing applications such as Lidar. Finally, we will explain some of the applications and advances in the field of Lidar. This article is intended to give a general overview of light in remote sensing while focusing on what is feasible today.

9.2 Historical Overview

The beginning of remote sensing is most likely the invention of triangulation, a technique to measure the distance to some location (possibly remote and inaccessible). Essentially, it involves selecting two positions whose separation is known and measuring the angle subtended at each position by the other position and by the remote location (via light coming from the remote location). Consequently, one has a triangle whose vertices are the two positions and the remote location; the length of one side is known and two angles have been measured, so simple geometry gives the distances to the remote location from each of the two positions. The ancient Greeks already knew that triangles can be used to estimate distances.

Thales had used such a technique in the sixth century BC in order to estimate the height of the Pyramids in Egypt. He simply compared the length of the Pyramid's shadow with his own shadow arriving at the ratio between the height of the Pyramid and his own height. While this knowledge was later somehow lost in Europe, it was noticed in ancient China around 200 AD that triangulation is essential to accurate cartography. The method of using triangles to measure distances was reintroduced to Europe by Arabic scholars around 1000 AD. During the sixteenth century triangulation was widely used in local cartography. The next big step forward was accomplished by Snell in the 1600s; he was the first to establish the required adjustments to the method in order to compensate for the Earth's curvature. Accordingly, local cartography was entirely based on triangulation and many countries established triangular networks over their entire landmass. Today, triangulation on a nationwide scale has been replaced by the global positioning system (GPS). In GPS, satellites continuously send timing information to the GPS receiver. As the exact positions of the satellites are known, the receiver can figure out the runtime differences for the signals to its location and thus determine the position of the receiver relative to that of the satellite. Thus, GPS is basically a modern variant of triangulation.

9.2.1 Speed of Light

In a sense, the measurement of the speed of light historically constituted a form of remote sensing. The ancient Greek philosopher Empedocles had already suspected that the speed of light is finite. However, at the time the theory that the eye actually sends out light was more common and so there was no real need for the notion of the speed of light. The Arabic scholar Alhazen published the first long treatise on optics and postulated that the eye actually only receives light. He then correctly argued that light has a finite speed and that in fact it travels slower in dense media. Since there was no clear idea how to experimentally prove that the speed of light was finite, over the centuries a lot of arguments were exchanged for either view. The first one to experimentally prove that light has a finite speed was Ole Rømer, a Danish astronomer, in 1676. He used an astronomical method in order to arrive at the conclusion that the speed of light was finite by observing the motion of the innermost moon of Jupiter, Io, on its orbit around Jupiter. Based on Rømer's observations, Huygens determined a value of the speed of light which differed from today's value by approximately one third. More refined techniques for measuring the speed of light were developed; these used a long optical path and rotating mirrors that would reflect the light back to the observer if the mirror had rotated to the right angular position by the time the light arrived at it. For a long time this had been the most accurate method until superseded by independent measurements of the wavelength and frequency of the light. The product of these quantities yields the speed of light.

Today, the speed of light has a defined value adopted in 1983. Since the invention of the atomic clock, time is the most accurately measured physical quantity. Consequently, the definition of length arrives at the same level of precision when the speed of light is fixed and distance is defined via the product of time and speed.

9.2.2 Fraunhofer and the Invention of Remote Sensing

Remote sensing in its modern meaning was unknowingly established by Fraunhofer. In 1801, Fraunhofer survived a collapse of the glass-making workshop in which he was working as an apprentice. The Prince Elector of Bavaria was so

elated to find at least one survivor that he donated money to the orphan Fraunhofer who was 14 years old at the time. Fraunhofer invested the money in books and learned in the following years to produce optical glass of previously unknown purity and quality. He further invented a spectroscope, essentially a predecessor of today's spectrographs, that can analyze light for its spectral content. In 1814, he observed almost 600 dark lines in the white solar spectrum—far more than Wollaston had observed a couple of years earlier and independently from Fraunhofer. Later Bunsen and Kirchhoff realized that these lines actually were absorption lines of gases in the solar atmosphere. Kirchhoff recognized that a particular set of lines was unique to one special element just like a fingerprint is for a human being. This essentially established spectroscopy as a science and constitutes the first example of remote sensing of the gases in the solar atmosphere. In honor of Fraunhofer, these absorption lines are called Fraunhofer lines. This very specific absorption of any gas (atoms or molecules) will prove very useful when we discuss active remote sensing schemes below.

9.2.3 Passive Remote Sensing

The invention of photography in combination with the ability to fly in unmanned or manned vehicles led to the birth of a broad range of passive remote sensing. The first example is aerial photography. Needless to say, this was very important for military purposes; but it was soon realized that other very valuable information could be extracted from the pictures. This is true in particular for the much higher quality images available from high-flying planes and nowadays satellites. The very sensitive detection devices and optics on board modern satellites allow a variety of remote sensing applications. But, since this article is focussed on optics in remote sensing, the discussion will omit techniques applying acoustic or radar based methods. The most common objectives in the passive satellite based remote sensing programs include meteorological observations for weather forecasting, predictions of hurricane movements, sea surface temperature distributions, military applications and reconnaissance, topographic mapping (stereo photography), or applications in mineralogy, biology, and archaeology.

One of the more sophisticated techniques is hyperspectral imaging in which a variety of images in different spectral regions are obtained; these give a complete picture of the reflective behavior of the Earth's surface. Thus, information such as plant coverage, snow coverage in mountains or the Arctic, and ground-level humidity can be extracted from the data. Such information is especially useful in, for example, analyzing the environmental impact of human activities, or in monitoring other environmental changes.

9.3 The Development of the Laser for Active Remote Sensing

The big leap from passive to active remote sensing required an appropriate light source capable of sending collimated light beams over large distances. In 1960 such a light source, the laser, was operated for the first time; it was invented by T. Maiman after C. Townes and A. Shalow had shown in 1958 that it was theoretically feasible. The acronym laser stands for light amplification by stimulated emission of radiation. In 1918 Albert Einstein had investigated a different phenomenon associated with the interaction of light with matter. Light could be absorbed by an atom, i.e., if a photon, whose energy corresponded to the energy difference between the ground and an excited state of the atom, were to

interact with the atom, it could be annihilated and the atom would then be elevated to the excited state of higher energy. The reverse process of an atom in the excited state falling back down to the ground state would then lead to the emission of a photon. Essentially, there are two kinds of emission processes: spontaneous emission occurring by chance without any cause, and stimulated emission occurring when a photon of the correct energy difference interacts with an excited atom and stimulates it to emit. In the latter case, the final result is an atom in the ground state and two photons—the original one and the stimulated one; furthermore, the stimulated photon is an exact copy of the original photon. In essence, this is an amplification process. In the laser this process leads to a large increase in the number of photons; specifically, since the photons are reflected back and forth many times through the medium, many photons are generated. Since the probability an incident photon will be absorbed by a ground state atom is identical to the probability an incident photon will stimulate an excited atom to emit a photon, this laser process works when there are a larger number of atoms in the excited state than in the ground state. This condition is referred to as a population inversion. The many reflections are made possible by the fact that the medium is between two mirrors forming a resonator. One of the mirrors is slightly less reflective than the other so that a small amount of light leaks through it, leaves the laser resonator, and can be used for applications. There are three important properties of this light: First, since the resonator defines an axis of symmetry, the light is highly directed along this very axis; second, since the radiation is closely linked to an atomic transition, the light consists of a single frequency corresponding to that atomic transition frequency; and third, since the photons are generated in a stimulated emission process, the light is coherent. All three properties make up the very unique features of laser light and essentially make it ideal for our purpose of remote sensing. However, just the invention of the laser was not yet enough to fulfill all our needs.

The next necessary step was the invention of the so-called Q-switched laser, which followed in 1962 very soon after the invention of the laser. While a laser in itself can produce very powerful light, the amount of light emanating from it was not enough to perform remote sensing in the atmosphere. The "Q" in Q-switch stands for quality. When the medium of a laser placed inside a cavity is pumped by an energy source achieving population inversion, light is amplified as soon as the gain of the stimulated emission exceeds the losses of the cavity. Consequently, the overall energy in the system is reduced by the stimulated emission (lasing) leaving the medium in the cavity. However, the medium could potentially store much more energy if lasing did not occur.

So, what if at first the cavity was of low quality? Light is not reflected back and forth and no amplification takes place. In this case, almost all of the energy in the pump source is stored in the medium. Once this has happened, the cavity can be suddenly switched into a state of high quality. Now, all of the energy stored in the medium is deposited into a giant pulse with very high energy and a few nanoseconds duration, i.e., some billionths of a second. The sudden switch of the cavity's quality is performed by the Q-switch. In general, this is an electro-optic modulator that manipulates the polarization of the light by applying a short voltage pulse to it.

Inevitably, a pulsed laser has a larger linewidth than a continuous wave laser. The minimum bandwidth is given by the so-called Fourier transform limit. In general, however, a pulsed laser has an even larger bandwidth than this limit. But, since the transitions in typical trace gases are fairly well separated, this linewidth increase does not change the selectivity in detection of trace gases. As stated above, the typical pulse durations of Q-switched lasers are in the nanosecond regime. This duration actually determines the typical spatial resolution one can achieve via time-of-flight measurements.

The first laser in 1960 was based on a solid state material known as ruby. The first Q-switched laser was based on the very same material. Ruby as a laser material, however, has a serious drawback. It is only capable of generating laser light around a very well-defined frequency. In fact, most of the early lasers had this limitation, albeit at different wavelengths. Unfortunately, these available laser frequencies were not resonant with any of the transitions of the interesting gases for remote sensing. Thus, another step was necessary in the development of the laser as a valuable tool in remote sensing. The next advancement was the invention of the tunable laser, i.e., a laser whose output frequency could be changed so as to match the transitions of gases of interest. The first tunable laser was the dye laser invented in 1966 independently by Sorokin and by Schäfer. In a dye laser the laser medium consists of an organic dye dissolved in an organic liquid such as methanol and ethanol. In solution, the individual resonances of the dye broaden to a wide band that leads to a broad emission spectrum. By placing additional optical components in the cavity, the laser can be restricted to work at a particular frequency within this band. And, by slightly adjusting the alignment of the components, the output wavelength can be tuned over the entire emission band of the dye. Now, the output of the laser could be tuned to the exact transition needed for a particular gas to be detected. In the following years many dyes were found suitable for such lasers; they cover a broad range of different wavelengths from the IR range, through the visible spectrum, and into the UV regime. And, the Ti:Sapphire laser now provides a solid state alternative that is capable of generating any wavelength in the near IR range.

As we will see later, even shorter pulses can be advantageous for remote sensing. The reason is twofold. First, very short pulses have very high peak intensities that can be directly applied to non-linear detection schemes that are now both available and increasingly important for applications in remote sensing. Second, since pulsed lasers have a larger bandwidth, there is the possibility of detecting several different species at once. Unfortunately, Q-switching only provides pulses in the nanosecond regime, this is essentially due to a combination of the typical size of the laser cavities and the gain of the media involved. However, a laser resonator does not lase on any wavelength, but only on the so-called longitudinal modes. This is comparable to the oscillations of a mechanical string fixed at both ends. The length of the string is an integer multiple of half the wavelength of the possible oscillations; the same is true of the laser oscillations. Thus, in general, the spectrum of a pulsed laser consists of a superposition of these longitudinal modes. There are techniques to synchronize these different modes. When these modes all oscillate with the same phase, something remarkable happens: the radiation in these modes interferes constructively to form giant pulses. The more longitudinal modes are involved the shorter the duration of these pulses. Moreover, the giant pulses oscillate back and forth in the cavity and exit at the corresponding high repetition rate.

9.4 LIDAR

Lidar for active optical remote sensing has a broad range of important applications. Some specific applications to be discussed in the following include: (Sect. 9.4.1) the precision measurement of distances over ranges varying from a few meters to thousands of kilometers, (Sect. 9.4.2) measuring the speed of an object at a distance point, (Sect. 9.4.3) measuring sound speed as a function of depth in the ocean, (Sect. 9.4.4) measuring temperature as a function of depth in the ocean, (Sect. 9.4.5) detecting and identifying underwater objects (fish, mines, etc.), (Sect. 9.4.6) detecting trace impurities in the atmosphere, (Sect. 9.4.7) a quite recent development, a femtosecond-Lidar application for influencing

weather phenomena, and (Sect. 9.4.8) stand-off super-radiant spectroscopy. A few other important applications that require at least a brief mention include steering a laser beam by inducing refractive index gradients, measuring depth profiles of particulate backscattering in the ocean; obtaining broad areal depictions of the sound speed environment; unraveling sonar signals in regions of varying sound speed; collecting important input for weather forecasting and climate change studies; understanding the behavior of biological populations in the ocean as well as the interactions between oceanic physical and biological structures; and studying/mapping the atmosphere for gases, aerosols, clouds, and temperature.

9.4.1 The Precision Measurement of Distances

The distance d to an object can be measured by sending a short laser pulse to the object and then measuring the time t it takes for the reflected pulse to return. Since the pulse travels a round-trip distance $2d$ in time t, the distance d is given by

$$d = \frac{ct}{2}, \tag{9.1}$$

where c is the speed of light. In practice, one sends a series of pulses, measures the travel time t for each pulse with sub-nanosecond accuracy, and averages the results to then obtain d from Eq. (9.1).

This approach to measuring distances has developed a wide range of applications. It is, for example, very useful in construction and real estate; it essentially replaces the tape measure. Rather than two people with a tape measure to determine the size of a large room, one person with a laser rangefinder can quickly measure it to very high accuracy. Typical of rangefinders for this use is the Bosch Model GLR825 which can measure distances from 50 mm to 250 m with an accuracy of ±1 mm [1]; it presently sells for about $400. Use of a tape measure to determine the width of a 10 m wide room to this kind of accuracy (i.e., one part in 10,000) would be highly problematic.

At the other extreme of LIDAR distance measurements, is the determination of the distance from the earth to the moon (the mean value is 385,000 km). The astronauts placed retroreflectors (corner cubes that reflect incident light by 180°) on the moon during the first lunar landing in 1969; there have been several other retroreflectors placed on the moon since then. The time t for a light pulse to travel from the earth to those retroreflectors and back is then measured and the distance from the surface of the earth to the surface of the moon is determined using Eq. (9.1). Such measurements are quite challenging. As discussed by Dickey et al. [2], the area illuminated on the lunar surface due to the divergence of the transmitted laser beam is ~7 km diameter and the retroreflector only intercepts $\sim 10^{-9}$ of that area. Due to the diffraction/divergence of the retroreflected beam, a 1 m diameter telescope on the earth will only collect $\sim 2 \times 10^{-9}$ of it. These two factors lead to a signal collection that is only 2×10^{-18} of the initial laser beam intensity I_0. Other factors such as detector quantum efficiency and mirror reflectivities less than one lead to an overall observed signal of $\sim 10^{-21}\ I_0$. So, if the laser sends out 10^{19} photons in each pulse, the average observed signal would only be one retroreflected photon for every 100 pulses. Nevertheless, the earth–moon distance can be measured with such high accuracy (~1 cm) that the earth–moon system becomes a "laboratory for a broad range of investigations, including astronomy, lunar science, gravitational physics, geodesy, and geodynamics" [2].

Some additional examples in this wide range of applications for laser rangefinder measurements include:

1. Autonomous vehicles—they require knowledge of the distance to nearby objects [3, 4] in order to avoid collisions.
2. Military applications—if the distance to a target is so great that gravitational effects on the projectile must be taken into account when aiming at the target [5, 6], then knowledge of the distance is critical. The MARK VII military rangefinder is an example of a device that meets this need; it operates at ranges of up to 20 km with an accuracy of ±3 m [7].
3. Sports—in golf, the use of laser ranging can significantly improve hitting accuracy by providing an accurate distance to the target [8].
4. Archaeology—high resolution depth measurements and contour mapping at a site can reveal archaeological features that are otherwise hidden [9].
5. Sub-surface topographical measurements—similar to the archaeology application, the topology of reef substrates (that impact the biology of reef organisms) can be obtained using NASA's Experimental Advanced Airborne Research Lidar (EAARL) [10, 11].

9

9.4.2 Measuring the Speed of an Object at a Distance Point

If a laser beam is reflected back on itself from an object that is moving in either direction along the same line as the laser beam, then the frequency of the reflected light will be Doppler shifted. By measuring the frequency shift of the reflected light, one can obtain the component of the object's velocity parallel to the laser beam and also determine whether it is approaching or going away. If the object is moving perpendicular to the laser beam, there is no frequency shift in the retroreflected light; but, this component of the velocity could be measured by measuring both the distance and the changing angular direction to the object. The bottom line is that the frequency shift only gives the component of the object's velocity along the direction of the laser beam.

In practice, the system works just as with the rangefinder; a laser pulse is directed to a target and the reflected light is collected. The travel time can still be used to determine the distance to the target; but, in this case the reflected light is also analyzed in frequency to determine the Doppler shift.

To quantify the speed as a function of the frequency shift, recall that the observed frequency due to the motion of a source of electromagnetic waves relative to the observer is given by [12]

$$f = f_0 \sqrt{\frac{c+v}{c-v}}, \tag{9.2}$$

where f is the frequency measured by the observer, f_0 is the frequency in the rest frame of the source, c is the speed of light in the surrounding medium, and v is the relative speed of the source and observer—it is positive (negative) when the source is approaching (moving away from) the observer. Note, v is just the relative speed of source and observer; it does not matter whether the source, observer, or even both are moving.

Now consider the LIDAR application to determine the speed of a target. The laser is the source with frequency f_0, the target is the observer that sees a frequency f_T given by Eq. (9.2) (f on the left-hand side is replaced by f_T). The target is now the

source and reflects source light of frequency f_T back towards the laser; the laser position is now the observer and observes a return frequency f_R given by

$$f_R = f_T\sqrt{\frac{c+v}{c-v}} = f_0\sqrt{\frac{c+v}{c-v}}\sqrt{\frac{c+v}{c-v}} = f_0\left(\frac{c+v}{c-v}\right) \tag{9.3}$$

If $v \ll c$, this can be approximated as

$$f_R \approx f_0\left(1+\frac{2v}{c}\right), \tag{9.4}$$

and the frequency shift due to the Doppler effect is

$$f_R - f_0 \approx \frac{2v}{c}f_0 = \frac{2v}{\lambda_0}. \tag{9.5}$$

Suppose a target is moving with a speed $v = 5$ m/s (~11 miles/hr) and the laser has a wavelength $\lambda_0 = 500$ nm (~blue). Then, the Doppler frequency shift from Eq. (9.5) is

$$f_R - f_0 = 20 \text{ MHz}. \tag{9.6}$$

Measuring such a frequency shift with a good Fabry–Perot is straightforward; a more difficult problem is the laser bandwidth. For a Gaussian laser pulse, the Fourier transform limited time-bandwidth product is

$$\tau\,\Delta f \geq \frac{2\ln 2}{\pi} \approx 0.44, \tag{9.7}$$

where Δf is the frequency bandwidth and τ is the temporal width (both full width half maximum). Thus, in order to resolve the Doppler shift in Eq. (9.6), the temporal width of the laser pulse must be greater than $\tau = 22 \times 10^{-9}$ s. Of course, for targets moving at higher speeds, this becomes less of a limitation. If the target is moving at 50 m/s, the Doppler frequency shift is 200 MHz and the laser pulse would only be required to have a temporal width greater than 2.2 ns.

9.4.3 Measuring Sound Speed as a Function of Depth in the Ocean

A light pulse propagating in the ocean is scattered by density fluctuations that propagate with the speed of sound. This scattering process is called Brillouin scattering and the remote sensing application, called Brillouin Lidar, has been studied [13–15]. As before, the depth is determined from the travel time of the light pulse; the speed (of sound) is measured by observing the Brillouin frequency shift f_B in the backscattered light. The basic physics of the Brillouin scattering problem is shown in Figs. 9.1 and 9.2.

Figure 9.1 shows the sound wave fronts for sound waves of wavelength λ_S and wave vector $\vec{k}_S$. A light beam of wave vector $\vec{k}$ is incident at an angle $\theta/2$ with respect to the sound wavefronts. The scattered light has a wave vector $\vec{k}'$; but since $\left|\vec{k}'\right| \approx \left|\vec{k}\right|$ and the angle of incidence on the sound wavefronts is equal to the angle of reflection, the scattered light must be at angle θ with respect to the incident light beam. From the sub-diagrams in Fig. 9.1, it is clear from momentum conservation that the magnitudes of the wave vectors must satisfy

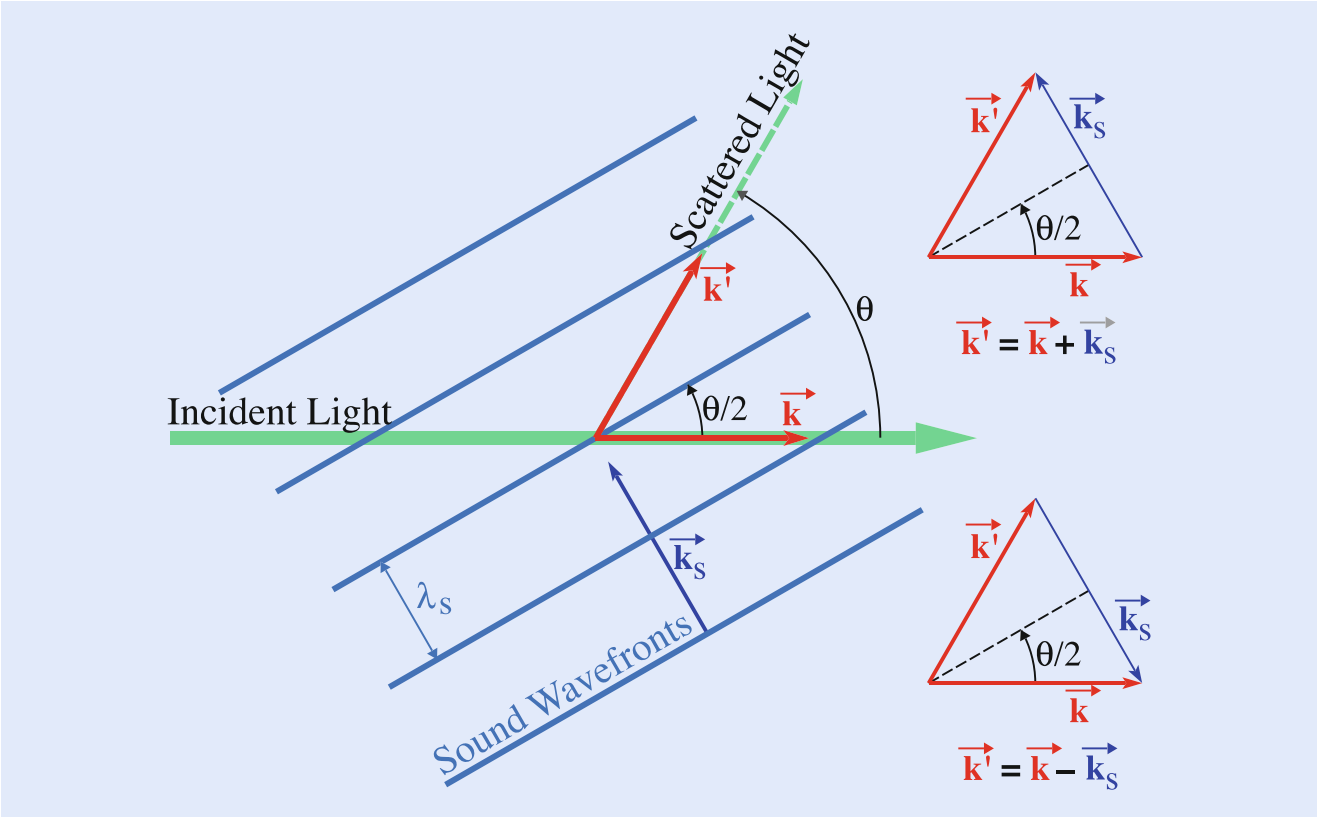

Fig. 9.1 Vector diagram for momentum conservation in Brillouin scattering

$$k_S = 2k \sin\frac{\theta}{2}. \tag{9.8}$$

Figure 9.2 shows a sound wavefront that moves a distance $v_S\Delta t$ in a time Δt. Point a on the initial sound wavefront becomes point b after the wavefront has moved the distance $v_S\Delta t$. Since the reflecting surface is a plane wavefront, the object and image distances must be the same. Thus, the distance of the source plane from point a equals the distance of the initial image of the source plane from point a. Similarly, the distance of the source plane from point b equals the distance of the image of the source plane from point b after the time Δt. From the inset in Fig. 9.2 it is clear the distance $V\Delta t$ that the image plane moves in time Δt must be given by

$$V\Delta t = 2\left(v_S\Delta t \sin\frac{\theta}{2}\right). \tag{9.9}$$

The relative speed V between the fixed observation plane and the moving image of the light source is therefore

$$V = 2v_S \sin\frac{\theta}{2}. \tag{9.10}$$

From Eq. (9.2), the observed frequency due to a source moving with a speed of magnitude V is

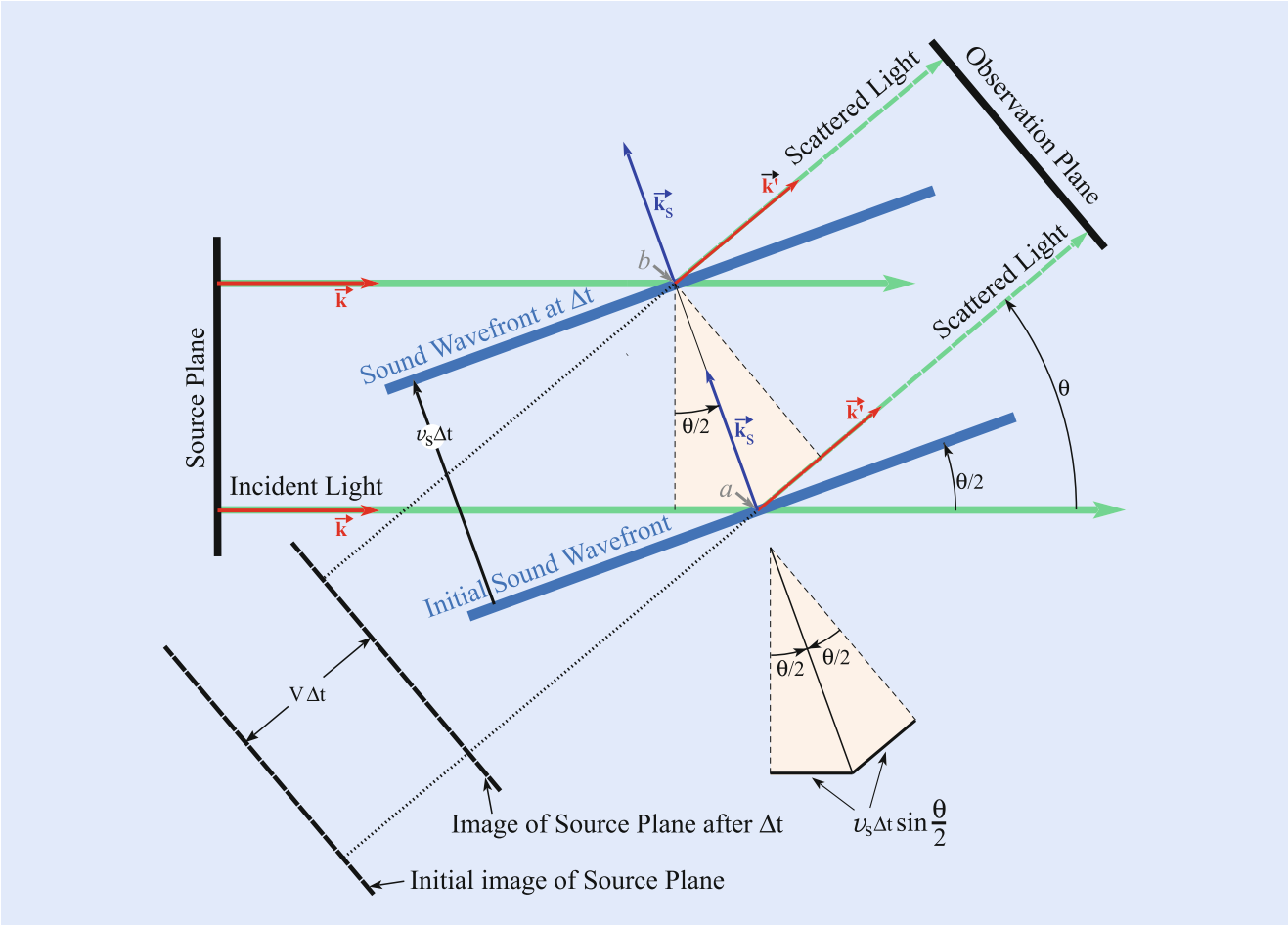

Fig. 9.2 Diagram for determining the Doppler shift

$$f_{\text{obs}} = f_0\sqrt{\frac{c \pm V}{c \mp V}} \approx f_0\left(1 \pm \frac{V}{c}\right), \tag{9.11}$$

where the approximation in the final step is that $V \ll c$. The upper (lower) sign corresponds to the image of the source plane moving towards (away from) the observation plane. The upper sign would be for $\vec{k}_S$, as shown in Fig. 9.2; the lower sign would be for $\vec{k}_S$, as shown in the second of the sub-diagrams of Fig. 9.1. The Brillouin frequency shift f_B is then

$$f_B = f_{\text{obs}} - f_0 = \pm\frac{V}{c}f_0 = \pm\frac{nV}{\lambda_0}, \tag{9.12}$$

where n is the index of refraction of the medium and λ_0 is the vacuum wavelength of the incident light. Inserting V from Eq. (9.10) gives

$$f_B = \pm v_S\, 2\frac{n}{\lambda_0}\,\sin\frac{\theta}{2}. \tag{9.13}$$

Note that for backscattering ($\theta = 180°$) with $n = 1$, Eq. (9.13) is identical to the Lidar frequency shift of an object moving at speed v_S, Eq. (9.5). Recall that the

wave vector has a magnitude given by $k = 2\pi n/\lambda_0$ for the incident light and $k_S = 2\pi/\lambda_S$ for the sound waves. Insert these in Eq. (9.8),

$$\frac{1}{\lambda_S} = 2\frac{n}{\lambda_0}\sin\frac{\theta}{2}, \tag{9.14}$$

and combine this result with Eq. (9.13) to obtain the interesting result,

$$f_B = \pm\frac{v_S}{\lambda_S} \equiv f_S, \tag{9.15}$$

that these two frequencies are identical, i.e., the Brillouin frequency shift of the incident light is identical to the frequency of the sound wave producing it.

The speed of sound waves is obtained by simply measuring the Brillouin shift f_B at some angle θ (generally backscattering at 180°) and using Eq. (9.13). For $\theta = 180°$, the sound speed is given by

$$v_S(S,T) = \frac{\lambda_0}{2}\frac{|f_B(S,T,\lambda_0)|}{n(S,T,\lambda_0)}$$

9

where the dependencies on salinity S, temperature T, and wavelength λ_0 have been explicitly shown.

For a typical value of the Brillouin shift, use Eq. (9.13) and take $\theta = 180°$, $\lambda = 530$ nm, $n = 1.33$, and $v_S = 1500$ m/s; the result is

$$f_B = \pm 7.5 \text{ GHz}. \tag{9.17}$$

In the oceans the Brillouin shifts are typically in the range of 7–8 GHz. In a Brillouin LIDAR, the sound speed actually being measured is the speed of high frequency (~7.5 GHz) sound waves.

As an example of a Brillouin spectrum, Fig. 9.3 shows experimental data for Brillouin backscattering by water using the second harmonic of a pulsed Nd:YAG laser [13]. The central peak (at relative frequency 0) is due almost entirely to elastic scattering by suspended particulates. The two peaks offset by ~7.5 GHz are the two Brillouin shifted peaks; they are due only to the water—suspended particulates do not contribute to them. The ratio of the intensity in the central peak to the total intensity in the Brillouin peaks is called the Landau–Placzek ratio [16, 17]. An interesting property of high purity water is that this ratio is so small;

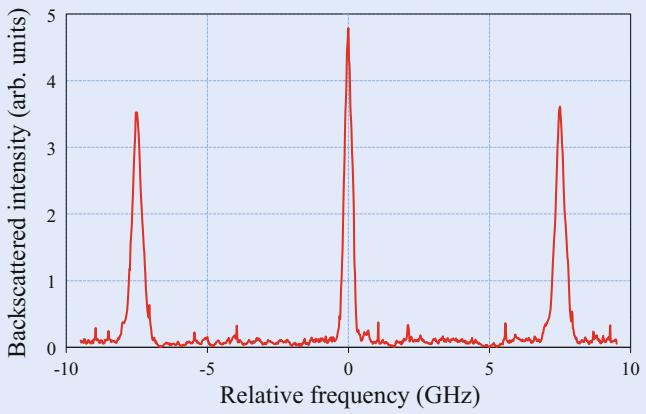

Fig. 9.3 Experimental data of Brillouin backscattering by water

experimentally and theoretically, it is a minimum and approximately 0–0.04 % at 4 °C, it increases with temperature and is approximately 2 % at 30 °C [17, 18].

A practical implementation of this Brillouin Lidar concept requires a receiver that collects light over an appreciable solid angle, that provides a high frequency resolution of the ~7 GHz frequency shifts, and that provides the measurements with ≈10 ns resolution over a time scale of several hundred nanoseconds (10 ns gives a depth resolution in water of ~1 m).

The first approach to achieve the required resolution might be a Fabry–Perot, but unfortunately the angular acceptance of a suitable Fabry–Perot is too small. For a Fabry–Perot with mirror separation d, the optical path difference between successive rays is $\delta = 2nd\cos\theta$, where n is the index of refraction of the medium between the plates and θ is the angle of incidence on the mirror surface inside the Fabry–Perot. At the transmission peaks the path difference is

$$\delta = 2nd\cos\theta = N\lambda_0, \tag{9.18}$$

where λ_0 is the vacuum wavelength and N is an integer which has its maximum value when $\theta = 0$.

If the free spectral range is $\Delta\lambda$ and the fullwidth at half maximum of the transmission peaks is γ, then the finesse F is defined as $F = \Delta\lambda/\gamma$. As the angle θ increases from the angle of a transmission peak, the path difference decreases and the transmission goes to zero, but rises again at the next transmission peak when the path difference has decreased by λ_0 and Eq. (9.18) is satisfied using $N-1$. If θ is increased from $\theta = 0$, then the maximum angle θ_m at which the transmission moves off the peak occurs when the path difference has decreased by a fraction of λ_0 given by $\gamma/\Delta\lambda$,

$$2nd\cos\theta_m = N\lambda_0 - \frac{\gamma}{\Delta\lambda}\lambda_0 = N\lambda_0 - \frac{\lambda_0}{\mathcal{F}} = 2nd - \frac{\lambda_0}{\mathcal{F}}. \tag{9.19}$$

Solving for θ_m gives

$$1 - \cos\theta_m = \frac{\lambda_0}{2nd\mathcal{F}}, \tag{9.20}$$

and expanding $\cos\theta_m$ for small θ_m gives

$$\theta_m \approx \sqrt{\frac{\lambda_0}{nd\mathcal{F}}}. \tag{9.21}$$

For typical values of $d = 1$ cm, $F = 40$, $n = 1$, and $\lambda_0 = 532$ nm, the angle is $\theta_m \sim 0.07°$; for reference, the angles for the transmission peaks are 0°, 0.42°, 0.59°, 0.72°, etc. The problem with $\theta_m \sim 0.07°$ can be understood by considering a practical situation in which the Brillouin Lidar receiver mirror has a diameter of 80 cm. The maximum divergence of Lidar signals collected by this mirror from a point source at a distance of 150 m would be 0.31°. This is already too large compared to 0.07°, but the problem is even worse. Specifically, a telescope would be required to reduce the diameter of the Lidar return from 80 cm to the few cm diameter of a practical Fabry–Perot; leading to a further significant increase in the beam divergence. The problem has been examined from several aspects by Hickman et al. [14].

The edge technique, a more recent approach, provided the capability to collect the Brillouin scattered light over an appreciable solid angle, to obtain the Brillouin frequency shift as a function of time with ≈10 ns resolution (i.e., 1 m depth resolution), and to do this over a time interval of hundreds of nanoseconds.

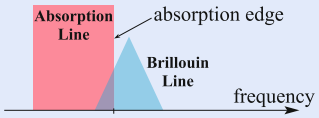

Fig. 9.4 The edge technique concept using an atomic/molecular absorption line

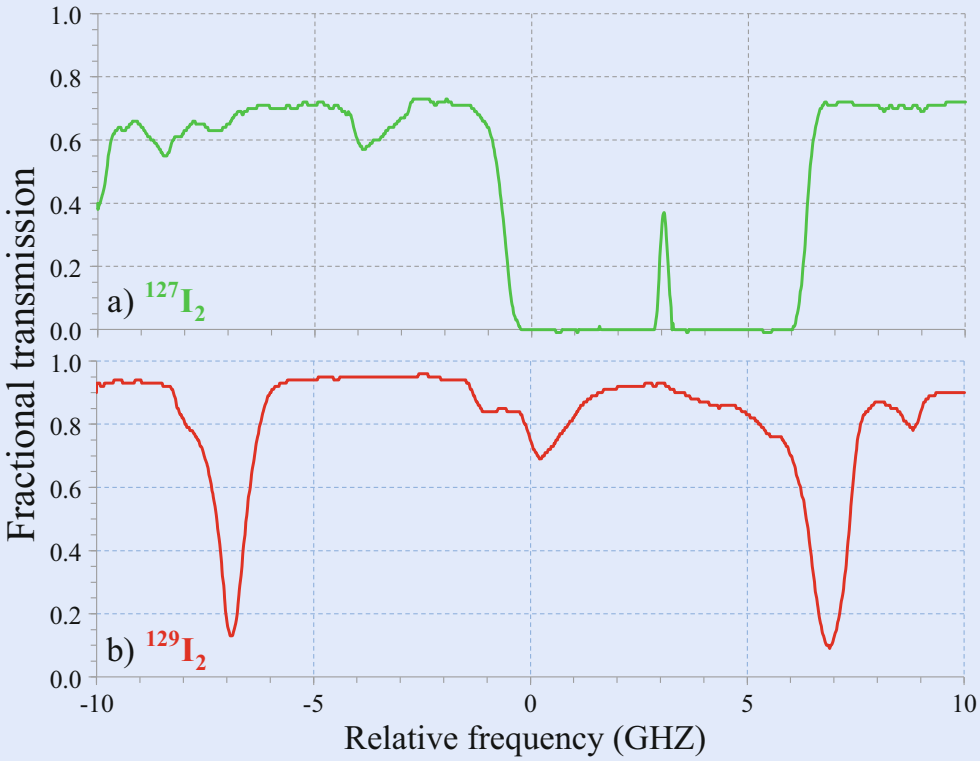

Fig. 9.5 Absorption spectra for the molecules (**a**) $^{127}I_2$ and (**b**) $^{129}I_2$; the zero on the relative frequency axis corresponds to an Nd:YAG laser wavelength of 532.38 nm

The approach is to use an atomic/molecular absorption line and to choose a laser frequency so that a Brillouin shifted component will lie on the edge of the absorption line. Figure 9.4 illustrates the concept with a fixed frequency rectangular absorption line and a triangular Brillouin line that partially overlaps the absorption line. The Brillouin Lidar return passes through a cell containing the absorbing gas that partially absorbs the Brillouin scattered light. The absorption decreases as the Brillouin shift increases, and vice versa.

Of course, the practical implementation is more complicated because there are two Brillouin lines that must lie on the edges of absorption lines; and there is also the central unshifted line due to scattering by particulates in the water that must be removed. Molecular absorption spectra were examined and a set of absorption lines that meet the requirements were found in $^{127}I_2$ and $^{129}I_2$; their absorption spectra are shown in Fig. 9.5.

The $^{127}I_2$ has strong absorption at the relative frequency zero (corresponding to the second harmonic of a Nd:YAG laser at 532.38 nm); it is used to remove the central peak. The outside edges of the two $^{129}I_2$ absorption lines are at a relative frequency of approximately ±7.5 GHz which would be the frequency of the

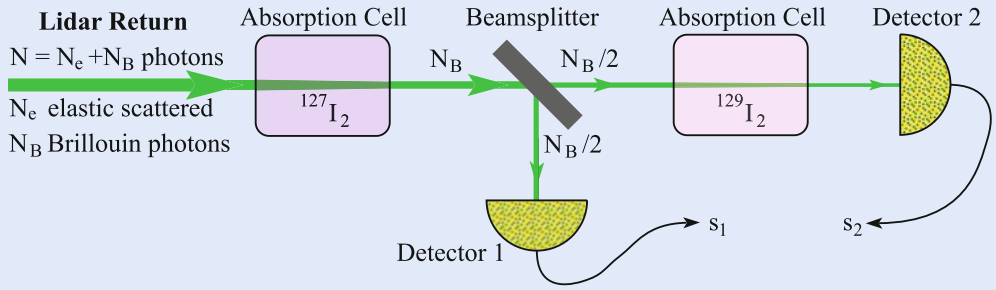

Fig. 9.6 Brillouin Lidar receiver using in $^{127}I_2$ and $^{129}I_2$ absorption cells

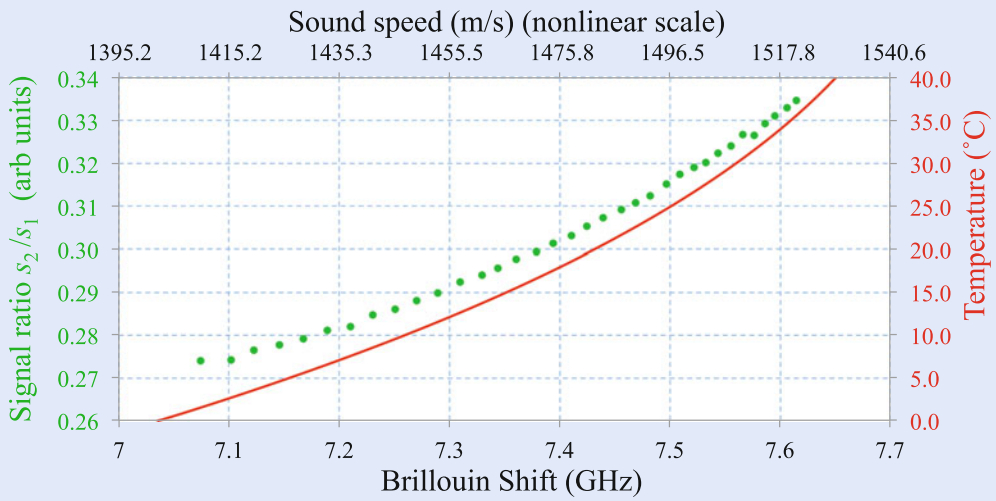

Fig. 9.7 Signal ratio s_2/s_1 (*dots*) and temperature (*smooth curve*) as a function of the Brillouin shift for pure water ($S = 0$); note that the ratio s_2/s_1 is on an arbitrary scale

Brillouin scattered peaks for typical conditions of temperature and salinity in the oceans and other natural waters.

A Brillouin Lidar receiver that implements the edge concept using these molecular absorption lines is shown in Fig. 9.6. The Lidar return first passes through a $^{127}I_2$ absorption cell that removes the central component and leaves only light that has been Brillouin scattered. Half of this light is then sent to a detector to obtain a reference signal s_1 for the total Brillouin scattered light. The other half passes through a $^{129}I_2$ absorption cell that absorbs a fraction of the Brillouin scattered light based on the extent to which the Brillouin lines overlap the $^{129}I_2$ absorption lines; it provides a signal s_2. After calibration, the ratio s_2/s_1 provides the Brillouin shift.

The efficacy of the system shown in Fig. 9.6 is demonstrated by its application to obtain the data in Fig. 9.7 which shows the measured ratio of s_2/s_1 (*dots*) as a function of the Brillouin shift at the laser wavelength, $\lambda_0 = 532.57$ nm, and salinity $S = 0$. The sound speed at each Brillouin shift marker is shown at the top of the plot; this scale is not quite linear because of the temperature dependence of the index of refraction. In practice, the temperature was varied and used to calculate the resulting Brillouin shift and sound speed at each data point [19]. The relation between temperature and Brillouin shift is also shown in Fig. 9.7 (smooth curve).

The use of the edges of molecular absorption lines was the first approach to the edge filter concept. But an especially promising approach is an excited state Faraday anomalous dispersion optical filter (ESFADOF) [20–22]. Basically, an absorption cell containing an atomic vapor is placed between crossed polarizers and in a strong magnetic field. The high anomalous dispersion in the vicinity of the absorption line rotates the polarization so some fraction of the light (based on its frequency overlap with the edge of the absorption line) passes through the second of the crossed polarizers. The ESFADOF can provide sharp absorption edges at the desired frequencies by adjusting the strength of the magnetic field. There has already been considerable progress made with this concept using the 543.3 nm transition ($5S_{1/2} \rightarrow 8D_{5/2}$) between excited states in Rubidium [23].

Stimulated Brillouin scattering (SBS) has also been used to measure Brillouin shifts [24, 25]. This approach gives a larger signal and since the source of SBS is small, the scattered light can be collimated to within the acceptance angle of a Fabry–Perot. The latter provides the spectral distribution of the SBS and hence a measurement of the Brillouin linewidth; this could be especially useful because at temperatures below 10 °C the Brillouin linewidth has a strong dependence on temperature [26]. SBS does not produce the anti-Stokes line, but its serious drawback is that it makes a measurement at one specific depth where the incident beam is focused to sufficient intensity to produce SBS. Consequently, depth profiling of sound speed requires refocusing of both the laser transmission and the receiver for each depth. In another application, SBS has recently been used to measure the bulk viscosity of water [27]; a measurement that had initially been demonstrated with spontaneous Brillouin scattering [28].

In summary, the very real possibility of sound speed profiles in the top 100 m of the oceans promise vital information to oceanographers, biologists, environmentalists, the military, and others. Aircraft could be used to rapidly obtain sound speed profiles from which the sound speed structure could be determined for large areas of the upper 100 m of the ocean. Knowing this structure would have many important applications; it could, for example, provide information about acoustic surface ducts and their temporal changes.

9.4.4 Measuring Temperature as a Function of Depth in the Ocean

Since over 70 % of the earth's surface is ocean, its temperature distribution on the surface and throughout the top mixed layers plays a major role in our weather and in forecasting our weather. Those temperature distributions in the upper-ocean mixed layers are also of major importance to understanding the physical and biological behaviors of the ocean. Fortunately, experimental depth profile measurements of the Brillouin shift can be converted to depth profiles of the temperature. Actually, this is already clear from Fig. 9.7—a given ratio s_2/s_1 (*black dot*) corresponds to a unique Brillouin shift (*bottom* axis), a unique sound speed (*top* axis), and a unique temperature (the temperature given by the *smooth curve* for that unique Brillouin shift and sound speed). It is also clear from Eq. (9.13), which in analogy with Eq. (9.16), can be written as

$$f_B(S, T, \lambda_0) = \pm 2 \frac{n(S, T, \lambda_0) v_S(S, T)}{\lambda_0}. \tag{9.22}$$

Since λ_0 is known, if f_B is measured, then Eq. (9.22) is a relationship between salinity S and temperature T. If salinity is known to within 0.1 %, a theoretical analysis shows that an uncertainty of 1 MHz in the Brillouin shift measurement corresponds to a temperature uncertainty of approximately 0.07 °C [19]. If the

value of salinity is based on an historical compilation of data [29], it can be expected to be accurate to within a standard deviation of about 1 %; with a 4 MHz uncertainty in the Brillouin frequency shift, the temperature uncertainty would be approximately 0.5 °C [19] (a smaller uncertainty in the Brillouin frequency shift would not have much effect on the temperature uncertainty).

For simplicity, the above discussion neglected pressure effects, but they are fairly easy to include when needed. In principle, the pressure P affects both the index of refraction $n(S,T,\lambda_0,P)$ and the sound speed $v_S(S,T,P)$; but the effects of pressure on the index of refraction are essentially negligible—at 0.0 °C the index increases by less than 0.015 % for a pressure increase of 10 atm [30]. However, pressure can have significant effects on sound speed; it has been well documented and an empirical equation for the dependence is available [31]. This equation must be used in the above calculations for $v_S(S,T,P)$ when the pressure differs from 1.0 atm.

9.4.5 Detecting and Identifying Underwater Objects (Fish, Mines, etc.)

There is an interesting and dramatically simpler version of the Brillouin Lidar that provides the capability of detecting and possibly identifying underwater objects [32, 33]. The point is that the Brillouin Lidar return consists of a central peak due to elastically scattered light and two Brillouin shifted side peaks. Those side peaks only occur if light is being scattered by water at the depth of observation. If there is anything at that depth other than water, the side peaks will not appear.

To detect and identify an underwater object, the laser is tuned to, for example, a strong I_2 absorption line that is chosen based on the condition that I_2 has negligible absorption in the spectral region between 7 and 8 GHz on either side of that absorption line. The Lidar return is then passed through a cell containing I_2 vapor where all elastically scattered light is removed from the Lidar return; only Brillouin scattered light remains. If there is something other than water at the observation depth, there is no light in the Lidar return. It does not matter what that something is, if it is not water, there is no light.

In practice, the Lidar return would pass through range gate optics to define the observation depth in the water, then through the I_2 cell to absorb all elastically scattered light, and then into a camera. The camera would produce a relatively uniform picture if nothing is in the water. But if there is, for example, a fish at the observation depth, the picture would be uniform except for a black region corresponding to the outline of the fish. For a single laser shot, the problem would be for the camera (or array detector) to collect enough light to make a good picture.

9.4.6 Trace Gas Detection

As we have seen earlier, the principle of Lidar can be used to accurately measure distances. Combining this capability with the very specific absorption features of gases provides a method to determine trace gas concentrations in the atmosphere. The idea is simple: tune the pulsed laser to the resonance frequency of the trace gas of interest and fire a short pulse of laser light into the atmosphere. The laser will be scattered back towards the sender. The time of flight of the backwards scattered light will yield the distance at which the pulse was scattered. In this way, a short pulse of nanosecond duration will be broadened to microseconds. But the light returning in a particular nanosecond slice within this broader pulse returns from a

well-defined distance. A requirement for this to be true is that the scattering cross-section be small enough such that there are no multiple-scattering events. If there were any, ambiguities in the return time would be introduced. When a certain amount of the trace gas is found in the path of the laser radiation, the light is absorbed more efficiently, indicating that indeed there is a certain amount of the trace gas in the path. In the returning pulse the trace gas would manifest itself as a reduction in the signal. As an example, consider the trace gas to be present only at a height of 10–15 km then obviously light coming back very early, i.e., from heights less than 10 km, no absorption would be present. The same is true for the return signal from heights above 15 km, but of course this light also has to propagate twice through the absorbing layer. Thus, a reduced signal would be observed in the return signal starting at times corresponding to a distance of 10–15 km. This reduction is stronger than the regular signal decay due to a longer path through the atmosphere. However, there is a serious problem. What if clouds are present at a height of 5–10 km? Clearly, the clouds lead to increased levels of scattering. Less light returns to the observer, and the observer not knowing about the clouds would attribute the absence of the signal to absorption, i.e., the presence of the trace gases at a height of 5–10 km as well. Fortunately, there is a solution to this. The technique is called DIAL or DIfferential Absorption Lidar. Essentially, it constitutes a slight modification of the laser system. Instead of just sending out radiation at one wavelength, the laser system now generates radiation at two wavelengths: one right on resonance with the trace gas as before and one slightly off the resonance such that this second beam is not absorbed by the trace gas. The idea is that any cloud in the atmosphere will influence the two wavelengths in the exact same manner. But the trace gas only absorbs radiation at one of the wavelengths. Thus, the difference in the two signal strengths is only caused by the presence of the trace gas. The effect of clouds would show up in both components and could thus be identified as being caused by clouds or any other scatterer.

9

It is easily conceivable that these types of measurements are quite complex and many challenges had to be met. As an example we want to discuss two issues. First, it would be ideal to make these types of measurements irrespective of the time of day. However, during daytime there is a lot of background radiation due to the sunlight; it easily swamps the small fraction of backscattered light. Thus, it was necessary to develop techniques to suppress the daylight. The solution was essentially narrow bandwidth filters that suppress the very broad spectral content of the sunlight without attenuating the returning laser light. While this constitutes a technical problem, the second issue is more fundamental in nature. It is the so-called inverse problem. Despite the fact that two wavelengths are used for the DIAL system, many effects can contribute to a certain return signal. It might be clouds, water droplets, snowflakes, ice, aerosols, very small volcanic debris from an eruption, etc. Moreover, the concentration distribution of a trace gas might be more complicated than indicated in our example. Thus, the unambiguous extraction of the actual atmospheric layering from the data is actually very complex and intricate. Bohren and Huffman have compared this problem in their book [34] on absorption and scattering by small particles to the problem of a knight hunting a dragon: it is actually quite straightforward to recognize the footprint of a dragon when seeing the dragon; it is very hard to conclude what the dragon might look like from just seeing its footprints.

The DIAL technique was developed in the early 1970s and 1980s as a method of sensitive trace gas detection in the atmosphere. At first DIAL was used to monitor many air pollutants and later it was used to monitor the depletion of the ozone layer. In principle, ozone can be detected using passive remote sensing techniques aboard satellites. The disadvantage is, however, that only the cumulative concentration can be measured. Any height information is lost. While this

height information can be extracted via balloon measurements, the laser based DIAL technique provides data much faster, more reliably and up to higher altitudes than the balloon based measurements; it is the superior approach.

9.4.7 Femtosecond-Lidar Application for Influencing Weather Phenomena

As noted earlier, a short pulse has a very large spectral bandwidth; hence, more than one trace gas species could potentially be detected simultaneously. Different spectral parts of the pulse would be absorbed by different species, and one laser with sufficiently short pulses should be able to simultaneously detect an entire range of trace gases. When researchers from France and Germany tried this for the first time at a relatively short distance, the technique indeed worked. However, when they directed the laser into the atmosphere, they discovered a surprise. Instead of a well-defined absorption at particular frequencies, they observed a bright white light extending a few hundred meters into the air. By beam steering and choice of laser parameters the researchers were able to move this channel to a variety of different locations. A thorough analysis revealed that the observation was actually a plasma channel forming due to the high intensity of the pulsed laser. The laser would ionize the air, producing a plasma state of free electrons and ions. The white light then originates from the ions and electrons recombining. In principle such a plasma state should make the laser diverge rapidly due to the contributions of the free electrons to the index of refraction. However, there is a focusing effect that counterbalances it so that propagation of the plasma channel is, in fact, relatively stable over a large distance. This self-focusing of a high intensity laser is known as the Kerr-effect. For high intensities the index of refraction has a non-linear contribution proportional to the intensity of the pulse. Since laser beams usually have a profile with higher intensity in the middle, the index of refraction is higher in the center; this leads to a focusing of the beam. Consequently, the two effects cancel each other and literally form an artificial lightning strike moving up into the atmosphere. Immediately, this sparks the creativity of a physicist. What if such a laser could be used to "direct" a natural lightning strike in a thunderstorm? Instead of more or less random lightning strikes, where it hits could be selected by essentially sending the artificial lightning strike towards an area where the next natural lightning strike is suspected. First experiments already hint at this becoming a reality in the near future. In thinking even further ahead, it is conceivable that using such a plasma channel could produce rainfall from clouds. Today, clouds are seeded by silver iodine in order to improve rain precipitation. In the future, it might become possible to just use such a femtosecond laser system to make rain from a cloud.

9.4.8 Stand-Off Super-Radiant Spectroscopy

Stand-off super-radiant spectroscopy is a promising remote sensing technique that is far more sensitive than Lidar or DIAL [35]. Briefly, the idea for detection of a weak concentration of some species is to use laser pulses to provide optical pumping of the species at a distant location in such a way that it will actually send back a laser beam signal. This is achieved by sending out multiple pairs of pulses along the same path; one pulse in a pair has wavelength λ_1 and the other λ_2. There is a small time delay $\Delta\tau$ between the two pulses in a pair and if $\lambda_1 > \lambda_2$, then the λ_2 pulse must be in the lead. The idea is that due to atmospheric dispersion, the longer wavelength pulse λ_1 will move faster and catch up to the shorter wavelength pulse at a well-defined distance determined by $\Delta\tau$. The wavelengths λ_1 and λ_2 are

chosen so that when they both interact with a gas molecule of interest, the molecule will be driven into an appropriate excited state (the upper lasing level) via two photon pumping, or via some Raman process. So, for a given $\Delta\tau$, there will be a well-defined distant point where the molecules of interest will be excited and produce a gain region. By sending out a long sequence of pulse pairs in which $\Delta\tau$ steadily decreases for each pair, there will be a long sequence of these gain regions being created in a direction directly back to the observer. Basically, it is a gain swept amplifier that is lasing straight back to the observer.

This approach will make it possible to detect parts per million concentrations of dangerous gases at distances of several kilometers. An important application of the gain swept amplifier is to actually obtain backward directed lasing from the major constituents of air, N_2 and O_2 [36]. A photon from this backward lasing can combine with a photon from a forward propagating interrogation laser beam to produce a molecular excitation in some trace gas. Then, by measuring the absorption of the backward propagating laser beam as a function of the wavelength of the interrogation laser, the trace gas concentration can be quantified with great sensitivity. Finally, this backward directed lasing could be an important tool in astronomical adaptive optics [37]; it could provide an artificial guide star at any position in the sky.

9.5 Conclusions

Optics and in particular light in remote sensing has evolved in the past decades to be one of the most important applications for learning more about the environment in which we live. The variation of optical methods for remote sensing is very large; it spans the gamut from airplane and satellite based passive remote sensing platforms to active remote sensing using time-of-flight techniques. In active remote sensing, the development of the laser and subsequently the introduction of Lidar have led to particularly striking progress. Lidar can be used for a large variety of tasks that shape knowledge about our environment—ocean temperature, trace gas detection in the atmosphere, air pollution in cities, telemetry, and many other applications. Once more optics and light is demonstrating how important and fundamental it is to our lives.

References

1. Robert Bosch Tool Corporation (2015) Power tools for professionals GLR825. ► http://www.boschtools.com/Products/Tools/Pages/BoschProductDetail.aspx?pid=glr825-specs
2. Dickey JO, Bender PL et al (1994) Lunar laser ranging: a continuing legacy of the Apollo program. Science 265(5171):482–490
3. Guizzo E (2011) How Google's self-driving car works. IEEE Spectrum. ► http://spectrum.ieee.org/automaton/robotics/artificial-intelligence/how-google-self-driving-car-works
4. Whitwam R (2014) How Google's self-driving cars detect and avoid obstacles. Extremetech. ► http://www.extremetech.com/extreme/189486-how-googles-self-driving-cars-detect-and-avoid-obstacles
5. Army Test and Evaluation Command, Aberdeen Proving Ground, MD (1969) Laser rangefinders. Ft. Belvoir Defense Technical Information Center
6. Litz B (2014) Laser rangefinders; Chapter 16 in Modern advancements in long range shooting. Applied Ballistics LLC, Cedar Springs, MI
7. Northrop Grumman Systems Corporation (2013) MARK VII handheld eyesafe laser target locator. ► http://www.northropgrumman.com/Capabilities/MarkVII/Documents/markvii.pdf
8. Owen D (2011) Stuff I like: long-distance operators. Golf Dig 62(3):70–71
9. Pappas S (2013) Legend of lost city spurs exploration, debate. Live Science. ► http://www.livescience.com/37539-legend-ciudad-blanca-lost-city.html
10. Wright CW, Brock JC (2002) EAARL: a lidar for mapping shallow coral reefs and other coastal environments. In: Proceedings of the 7th international conference on remote sensing for marine and coastal environments, Miami
11. Brock JC, Wright CW et al (2004) LIDAR optical rugosity of coral reefs in Biscayne National Park, Florida. Coral Reefs 23:48–59
12. Young HD, Freedman RA (2014) University physics with modern physics. Pearson
13. Fry ES (2012) Remote sensing of sound speed in the ocean via Brillouin scattering. In: Hou W, Arnone R (eds) Proceedings of SPIE 8372. pp 8372071–8372078
14. Hickman GD, Harding JM et al (1991) Aircraft laser sensing of sound velocity in water: Brillouin scattering. Remote Sens Environ 36:165–178
15. Guagliardo JL, Dufilho HL (1980) Range-resolved Brillouin scattering using a pulsed laser. Rev Sci Instrum 51:79–81
16. Cummins HZ, Gammon RW (1966) Rayleigh and Brillouin scattering in liquids: the Landau—Placzek ratio. J Chem Phys 44:2785–2796
17. Rouch J, Lai CC et al (1976) Brillouin scattering studies of normal and supercooled water. J Chem Phys 65:4016–4021
18. O'Connor CL, Schlupf JP (1967) Brillouin scattering studies of normal and supercooled water. J Chem Phys 47:31–38
19. Fry ES, Emery Y et al (1997) Accuracy limitations on Brillouin lidar measurements of temperature and sound speed in the ocean. Appl Opt 36:6887–6894
20. Schorstein K, Scheich G et al (2007) A fiber amplifier and an ESFADOF: developments for a transceiver in a Brillouin-LIDAR. Laser Phys 17:975–982
21. Popescu A, Walther T (2009) On an ESFADOF edge-filter for a range resolved Brillouin-lidar: the high vapor density and high pump intensity regime. Appl Phys B 98:667–675
22. Rudolf A, Walther T (2012) High-transmission excited-state Faraday anomalous dispersion optical filter edge filter based on a Halbach cylinder magnetic-field configuration, Opt Lett 37:4477–4479
23. Rudolf A, Walther T (2014) Laboratory demonstration of a Brillouin lidar to remotely measure temperature profiles of the ocean. Opt Eng 53:051407, 1–9
24. Shi J, Li G et al (2007) A lidar system based on stimulated Brillouin scattering. Appl Phys B 86:177–179
25. Shi J, Ouyang M et al (2008) A Brillouin lidar system using F–P etalon and ICCD for remote sensing of the ocean. Appl Phys B 90:569–571
26. Fry ES, Katz J et al (2002) Temperature dependence of the Brillouin linewidth in water. J Mod Opt 49:411–418
27. He X, Wei H et al (2012) Experimental measurement of bulk viscosity of water based on stimulated Brillouin scattering. Opt Commun 285:4120–4124
28. Xu J, Ren X et al (2003) Measurement of the bulk viscosity of liquid by Brillouin scattering. Appl Opt 42:6704–6709
29. National Oceangraphic Data Center (NODC), User Services Branch, NOAA/NESDIS E/OC21 (1993) Oceanographic station profile time series
30. The International Association for the Properties of Water and Steam (1997) Release on the refractive index of ordinary water substance as a function of wavelength, temperature and pressure. ► http://www.iapws.org/relguide/rindex.pdf

31. Grosso VAD (1974) New equation for the speed of sound in natural waters (with comparisons to other equations). J Acoust Soc Am 56:1084–1091
32. Fry ES, Kattawar GW et al (2000) System and method for detecting underwater objects. Texas A&M University, Patent# 6388246
33. Gong W, Dai R et al (2004) Detecting submerged objects by Brillouin scattering. Appl Phys B 79:635–639
34. Bohren CF, Huffman DR (1983) Absorption and scattering of light by small particles. Wiley, New York
35. Kocharovsky V, Cameron S et al (2005) Gain-swept superradiance applied to the stand-off detection of trace impurities in the atmosphere. Proc Natl Acad Sci U S A 102:7806–7811
36. Hemmer PR, Miles RB et al (2011) Standoff spectroscopy via remote generation of a backward-propagating laser beam. Proc Natl Acad Sci U S A 108:3130–3134
37. Wizinowich PL, Mignant DL et al (2006) The W. M. Keck observatory laser guide star adaptive optics system: overview. Publ Astron Soc Pac 118:297–309